Lab on a Chip

Accepted Manuscript

ROYAL SOCIETY OF CHEMISTRY

www.rsc.org/loc

A Bubble-based Microfluidic Gas Sensor for Gas Chromatographs

Ashrafuzzaman Bulbul and Hanseup Kim

Electrical and Computer Engineering, University of Utah, Salt Lake City, Utah 84112

United States

Abstract:

We report a new proof-of-concept bubble-based gas sensor for a gas chromatography system, which utilizes the unique relationship between the diameters of the produced bubbles to the gas types and mixture ratios as a sensing element. The bubble-based gas sensor consists of gas and liquid channels as well as a nozzle to produce gas bubbles through a micro-structure. It utilizes custom-developed software and an optical camera to statistically analyze the diameters of the produced bubbles in flow. The fabricated gas sensor showed that five types of gases (CO_2, He, H_2, N_2, and CH_4) produced (1) unique volumes of 0.44, 0.74, 1.03, 1.28, and 1.42nL (0%, 68%, 134%, 191%, and 223% higher than CO_2) and (2) characteristic linear expansion coefficients (slope) of 1.38, 2.93, 3.45, 5.06, and 5.44nL/(kPa/μLs^{-1}). The gas sensor also demonstrated that (3) different gas mixture ratios of CO_2:N_2 (100:0, 80:20, 50:50, 20:80 and 0:100) generated characteristic bubble diameters of 48.95, 77.99, 71.00, 78.53 and 99.50μm, resulting in a linear coefficient of 10.26μm/μLs^{-1}. It (4) successfully identified an injection (0.01μL) of pentane (C_5) into a continuous carrier gas stream of helium (He) by monitoring bubble diameters and creating a chromatogram and demonstrated (5) the output stability within only 5.60% variation in 67 testing over a month.

Introduction:

Miniature gas sensor devices for detection and analysis of gas compositions have recently attracted increasing interests due to their strong potential in understanding and resolving societal issues in various fields, including healthcare, occupational safety, and industrial processes. For example, portable monitoring of a wide range of toxic gas components in the 10,800 to 18,000 liters of gas that humans inhale on a daily basis [1] would provide clear insights into some respiratory diseases including asthma, emphysema, lung cancer, and myocardial infection [2-3], vaguely known to be related to air pollution. Distributed gas detection tools would allow community-level sensing and reaction in highly-populated urban areas that experience worsening air quality every year [4-5], as well as simultaneous increase of

respiratory diseases [3]. In the last few decades, the development of a variety of miniature gas sensors has been rigorously pursued in order to efficiently identify gas compositions that typically exist in an enormous variety (>180 toxic gases [6] and their mixtures).

Among advances in various miniature gas sensor devices, the development of a micro gas chromatography (μGC) system has been particularly noted because of its wide detection ranges. Unlike stand-alone gas sensors, a μGC system 'pre'-separates multiple gas compounds over time by incorporating a separation column [7-10] such that a sensor device needs to identify only one gas type at any time-scale thus without being overwhelmed by the simultaneous presence of multiple gas types. Such a pre-separation step allowed a GC system to detect more than 50 gas types [7-10], while a stand-alone gas sensor detected less than 10 gas compositions, even in an array or with the assistance of pattern recognition circuitry [11-15]. Considering that there exist more than 500 gas types of interest in science and engineering [6, 16], the large detection capacity of a GC system approach provides significant upgrades in gas analysis.

Despite notable advances in the miniaturization of a GC system, especially assisted by microelectromechanical systems (MEMS) technology, existing miniaturized GCs have not yet demonstrated the full integration of a long-term-stable, tiny-volume and easy-to-fabricate gas sensor device. Gas sensors, utilized in micro chromatography-systems, have employed either chemistry- or physics-based principles for gas detection, as listed in Table 1. Chemistry-based sensors, in the forms of chemiresistors [17-18], resonators [19-20], surface acoustic wave sensors (SAW) [21-22], metal oxide semiconductor (MOS) sensors [23-24], Fabry-perot sensors (FP) [25-26], and optical fiber sensor [11], suffer from significant output signal drifts and thus non-deterministic gas analysis over time, mainly due to the degradation of incorporated reactive materials. Chemistry-based sensors typically adopt a target-specific reactive film, vapor, or gas at its structural surface where the target gas molecules are adsorbed or temporarily absorbed to cause changes in either electrical, mechanical, chemical or optical properties for detection. Such reactive materials inevitably undergo oxidation or accumulation of target gas molecules, resulting in the changes of their properties overtime. Physics-based sensors avoid the use of reactive materials and thus the issue of output signal drifts overtime. Instead they directly measure physical properties that are not time-variable, such as mass, charges, conductance, and heat loss, by decomposing, burning, or navigating the target molecules into different angles or near a thin wire. However, such measurement typically requires bulky ancillary instruments that cannot fit into a miniaturized system or sophisticated structures that are currently difficult to fabricate in micro domain. Additionally, some physics-based sensors typically destroy the target samples during detection, often prohibiting some

potential post-detection analysis, such as the use of detected gases for biochemical effect evaluation [27-29]. Common physics-based sensors include electron capture detectors (ECD) [30], flame ionization detectors (FID) [31], mass spectrometry (MS) [32], and thermal conductance detectors (TCD) [33-34]. Mass spectrometry (MS) and flame ionization detectors (FID) require a high-performance vacuum pump that reaches 10^{-8} torr [32], while an electron capture detector (ECD) requires a radiation shielding structure [30], all of which have not yet been miniaturized into a chip-scale device. Recent development of thermal conductance detectors (TCD) in a micro column is notable [33-34]; however, these TCDs present relatively complex fabrication for mass production.

The aforementioned issues of a sensor component in current miniaturized GC systems can be resolved by utilizing gas bubbles as a non-variable, thus long-term-stable, physical sensing element for miniaturized, easy-to-fabricate and post-analysis-friendly gas detection. Unlike chemistry-based sensors, the production of bubbles from the pre-separated gas stream does not utilize reactive materials and results in non-drifting output signals. Unlike other physics-based sensors, it does not require complex fabrication, destruction of target samples, or ancillary instruments that cannot be miniaturized. Thus, it can avoid all the problems aforementioned. The production of bubbles has not yet been utilized as a sensing element for a gas sensor. Several previous studies have demonstrated that gas bubbles can be produced in a liquid stream in a micro channel, and that their resultant sizes are specifically determined by certain parameters of a specific gas type, such as tension, viscosity, flow rates, and pressure, utilizing only a single gas [35-49]. This study utilizes the variations in bubble size for different gas types in order to detect gases and produce gas chromatograms.

This paper reports the first time the use of gas bubble formation as a sensing element to distinguish gas types. Specifically, this paper discusses the design, fabrication, and testing results of the novel proof-of-concept bubble-based gas sensor, with two main areas of focus: (1) the characteristics of the produced bubbles, which depends on gas types and mixture ratios, in order to verify the feasibility of utilizing the bubble diameter as a sensing element and (2) the use of bubbles as a proof-of-concept sensing element and the initial resultant characteristics in terms of chromatogram production and long-term stability.

Concept of Bubble-based Gas Sensing:

Figure 1 explains the concept of the bubble-based gas sensor, where a gas is streamed into a liquid to produce bubbles while the sizes of the bubbles are monitored to generate the chromatogram. A gas

mixture is first separated in time and space into discrete groups of individual gases – C_5 (red), C_{10} (black), and C_{12} (blue) – by a conventional chromatographic column. The separated gas groups are then streamed into the liquid channel with the help of a carrier gas, e.g. helium (He), which is continuously flowing in a conventional gas chromatography system. The flow of the He carrier gas produces a train of uniform bubbles (gray) in a fixed size at a given nozzle dimension, as confirmed in previous articles [35-37, 50-51]. However, the injection of the separated gas targets (C_5, C_{10}, and C_{12}) into the He carrier gas changes the size of the bubbles depending on gas types and mixture ratios with the carrier gas. Thus by monitoring and plotting the variation of gas bubble sizes in reference to the background carrier gas bubble, a gas chromatogram can be established to identify gas peaks just as conventional gas sensors for a gas chromatograph.

Operation principle:

It is hypothesized that the variations in gas bubble diameter for different gas types are attributable to combined effects of multiple parameters, including gas density, gas solubility and gas diffusivity into the liquid, as studied in some bubble production research utilizing ultrasound [52-53]. Epstein reported an equation to describe the gradual gas dissolution process of a microbubble in liquid phase [52]:

$$\frac{dR}{dt} \propto -k\frac{C_s}{\rho}\left(1-\frac{C_i}{C_s}\right)\left\{\frac{1}{R}+\frac{1}{\sqrt{\pi kt}}\right\} \quad \text{----------(1)}$$

where R = bubble radius at time t, k = diffusion coefficient of the gas into the liquid, ρ = gas density, C_i = initial gas concentration in liquid, and C_s = saturated gas concentration in the liquid phase (i.e., gas solubility). This equation indicates that the bubble radius of a specific gas type depends on mainly three parameters: gas diffusivity k, gas solubility normalized by density C_s/ρ, and ratio of initial dissolved gas concentration to the saturation dissolved gas concentration C_i/C_s. As the gas stream enters into a nozzle, some portions dissolve into water based on their solubility before reaching the equilibrium to form a bubble and other portions further diffuse into the liquid. The equation implies that gases with higher solubility (C_s) will result in smaller bubble diameters, as indicated by the two terms C_s/ρ and C_i/C_s in equation (1), and that for gases with lower solubility the diffusion effect (k) may be more prominent in determining the bubble diameters. In order to investigate this, five types of gases were selected, representing various sets of solubility, solubility normalized by corresponding density and diffusivity, to produce bubbles, as shown in Table 2. Note that the equation utilized Laplace pressure to represent an existing bubble in liquid instead of its formation, thus requiring further modifications to precisely describe the microfluidic bubble production process at a nozzle as described in this study.

Structure and Fabrication:

The structure of the bubble-based gas sensor consists mainly of a gas flow channel, two liquid flow channels, a nozzle, and an outlet channel for bubble flow, as shown in Fig.2-(a-b). The gas flow channel introduces the gas stream between the two liquid flows that are provided by the liquid flow channels. At the intersection of both gas and liquid flows, the nozzle is located where the gas stream is cut into a train of discrete bubbles by continuous liquid flows (Fig.2-(c)). These channels consist of hydrophilic walls to maintain stable flow of liquid phase by wetting the channel walls, and their surface roughness is less than 1nm to avoid any disturbance in laminar flow through the channel. The channels are in 100's micro-meter ranges resulting in low Reynolds number (3×10^{-6} for liquid; 9.2 for gas phases), $Re = \frac{\rho u L}{\mu}$, for both liquid and gas phases to ensure the laminar flow through the channels. The width of the nozzle is designed to be narrower than those of the gas and liquid flow channels in order to reduce the size and increase the frequency of bubbles for higher precision measurement. The outlet channel is the path that the produced bubbles flow for optical measurement. The outlet channel extends the observation range through a meander shape within a compact footprint.

Fabrication was performed by molding individual PDMS layers containing a micro channel and stacking them with oxygen plasma bonding techniques through only one mask step (Fig.3). First, SU-8 2050 (MicroChem) polymer layer was utilized to construct a raised structure, a sacrificial channel mold for the fluid channels as well as the nozzle. The SU-8 pre-polymer was spin-coated at 2500rpm for 60s on top of a silicon wafer and subsequently cured at 65^0C for 3 minutes and 95^0C for 9 minutes. The resultant thickness of 38μm defined the heights. After being patterned with UV lithography at 350W and 30s, the SU-8 mold was post-baked at 65^0C for 2 minutes and 95^0C for 7 minutes to accelerate the cross linking mechanism in SU-8 and developed for 3-5 minutes in a SU-8 developer (MicroChem). On top of the fabricated mold, PDMS (Sylgard 186 Silicone Elastomer Kit), diluted in a curing agent at a 10:1 ratio, was poured and then cured at 65^0C for 6 hours. The same process was repeated to fabricate the top PDMS layer. The resultant widths of the fabricated gas channel, liquid channels, nozzle, and outlet channel were 200, 150, 40, and 600μm, respectively, and the height of all structures was 38μm. The length of the outlet channel was designed to be relatively shorter (15mm) to reduce the viscous resistance of the outlet channel, according to the Poiseuille equation as $R \cong \mu L/h^4$ where μ, L, and h are liquid viscosity, outlet channel length, and outlet channel height, respectively [36], resulting in the reduction of the required pressure to produce gas bubbles. The reduced pressure in turn decreased the bubble frequency within the limit of the given camera speed, the relationship of which was confirmed in previous studies by other research groups [35]. The designed volume fraction of the bubbles (the ratio of bubble to outlet channel

volumes) ranged between 0.33~0.37 in this particular study. On the PDMS layers, three I/O holes were drilled by a custom-made bio-puncher with a 20-gauge size (ID=0.6mm, OD=0.91mm), resulting in a final diameter of 600μm. The two PDMS layers were then bonded by exposing each layer under oxygen plasma using Dyne-A-Mite 3D treater and Enercon (120V and 4A for 30s), and stacking them on top of each other under pressure at room temperature. The bonded channel was immediately filled by a DI water to maintain the hydrophilic properties of oxidized PDMS walls. Each test was performed first by continuously flowing of liquids over 2-3 minutes in order to clear up any potential bubbles remaining at the wall of the channel. Within the tested flow rate range, bubble stiction was not observed in the micro channel. Note that the gas permeation through the PDMS walls can be estimated following the permeation flux equation [54]: $F = \frac{PA\Delta p}{d}$, where the gas-PDMS permeability (P), wall thickness (d), pressure difference (Δp), and effective gas-PDMS interface area are 10^{-9}gcm^{-3}s^{-1}(cmHg)$^{-1}$, 0.5cm, 7.5×10^{-1}cmHg and 1.1×10^{-4}cm^2, respectively. The calculated permeation rate is 1.7×10^{-13} g/cm^{2}s, which implies that one nitrogen gas molecule (4.65×10^{-23}g) through the given interface area would require 4.1×10^5 second to diffuse through the PDMS walls. Such estimated permeation time (4.1×10^5s) of gases through the PDMS walls is clearly much larger than the residence period (~1s) of each bubble flowing throughout the channel. Thus, the influence by gas permeation through the PDMS walls on the final bubble size during the measurement was neglected. The footprint of the fabricated device was 20×5mm^2 (Fig.2-(b)).

Testing Methodology:

Experimental testing mainly utilized the monitoring of the bubble diameters through video analysis in order to observe two aspects of this sensing process: (i) *the correlation of bubble size to gas types and mixture ratios* and *(ii) the sensing performance as a gas chromatography sensor in terms of detection and stability over time.* To generate bubbles, the target gases were supplied through a commercial GC instrument (Thermo Focus GC) at pressure of 6~20kPa, and liquid was provided in control by utilizing a syringe pump (KD Scientific, KDS-210). The produced bubbles were then video-recorded by an optical camera for detailed analysis.

Image analysis:

The optical camera-based unit was utilized to measure the diameters of flowing bubbles over a finite period of time (>60 sec). It consisted of a video camera (Edmund optics EO-1312M, speed 22 fps) coupled with a microscope (Mitutoyo) and a laptop for recording and analyzing the bubble. The utilized camera measured 400~550 bubbles per second, thus accommodating the bubble generation frequency under our experimental condition (~500 bubbles/s). The microscope incorporated 5X amplification

through a magnifying lens. The video recording was performed at a section of the full meandered channel that was 8mm away from the nozzle. The recorded video frames were then analyzed by a MATLAB-based custom program, resulting in statistical analysis data.

The developed MATLAB-based software processed an image analysis algorithm to precisely determine the size of the bubbles. First, the developed program divided the recorded video into grayscale frames of 1024×1280 pixels (Fig.4-(a)), where each pixel is equivalent to 1μm under a microscope with a 5X amplification factor. In the grayscale frame, each pixel of the whole frame was first assigned with corresponding darkness values, or pixel values, ranging from 0 (complete black) to 255 (complete white). Typically micro gas bubbles held dark or close-to-black colors in the pixel value range of 60~80, while the channel appeared bright or close-to-white colors in the pixel range of 150~170. Some space between the bubbles and the channel held gray colors. In order to clearly define the boundary and thus the size of each bubble, the grayscale frame was converted into a black-or-white (binary) frame by setting a threshold in the pixel values. For example, the pixels that hold the values below the threshold were converted into black, while the pixels above the threshold values were converted into white, as shown in Fig.4-(c). The threshold value was defined as the minimum pixel value that formed completely-filled and –circular shapes in all the bubbles within the frame. It was typically observed that 36.7% increase from the lowest pixel value (darkest color) successfully defined fully-circular shape for all the bubbles in the black and white image frame, as shown in Fig.4-(b). Thus, the threshold pixel value was set as 36.7% throughout the experiments. Then, the diameter of each binary image was determined by averaging the *x*- and *y*-axis diameters. Each bubble was then assigned with respective colors depending on the bubble sizes in order to visualize the bubble size distribution over frames (Fig.4-(d)). Finally, statistical data was generated on the counts and the diameters of the produced bubbles. Figure 4-(e) shows an example of statistical variation (3.1% variation of the mean diameter of 116.8μm) of 3042 helium gas bubbles over 210 frames in 10 seconds.

Characterization of bubble production:

To validate the feasibility of identifying gas types by monitoring bubbles as a sensing element, the variations in diameters of the produced bubbles were measured under various sets of gas types and mixtures. Additionally, pressure and flow rates were monitored to measure the characteristic conditions of the bubble production by locating a gas flow/pressure meter (Omega fma-1604a) at the inlet of the microfluidic device. The collected data were processed through the LabView program at the sampling frequency of 21Hz. Note that the bubble volume was measured at a fixed location, thus at a fixed time

point after its formation, for consistency, and did not consider its variations over time within the scope of this paper.

Gas types vs. bubble volumes:

To verify and compare the variations in the produced bubble volumes depending on gas types, five different gases (CO_2, He, H_2, N_2, and CH_4) were supplied to a microfluidic nozzle respectively while the diameter of the produced bubbles was monitored over a period of 1 minute. Then, the resultant gas diameters were converted to estimate volumes and then correlated to each gas type. Five different gas types were selected to cover the wide range of diffusivity and solubility of various gases, as mentioned in Table 2. The diffusivity covered from 1.49×10^{-5} (CH_4) through 1.88×10^{-5} (N_2), 1.92×10^{-5} (CO_2) and 4.5×10^{-5} (H_2) to $6.28\times10^{-5}cm^2/s$ (He), while the solubility of four gases (CH_4, N_2, H_2 and He) were similarly ranged between 0.009 and 0.0054 in contrast to that of CO_2 (1.716) [55-56]. The utilized liquid was a 52% glycerol/water mixture that held the viscosity of 6.1mPa.s [35-36]. The liquid flow rate and gas pressure were fixed at 22.17μL/s and 13.10kPa, respectively.

Gas types vs. p/q ratios vs. linearity:

The ratio of gas pressure to liquid flow rate, representing a control parameter of bubble volume, was adjusted from 0.39 to 0.59μL/s by increasing flow rates from 22.17 to 25.00, 27.84, 30.50, and 33.34μL/s at the fixed gas pressure of 13.10kPa while the diameters of the produced gas bubbles were monitored, in order to determine the linearity of the volume expansion coefficients for each gas. The linearity coefficients allow the prediction of the diameters of the produced bubbles under different flow conditions. The range of the selected liquid flow rates, between 22.17 and 33.34μL/s, was experimentally determined to ensure stable bubble generation at the given nozzle geometry. Below the liquid flow rate of 22.17μL/s, the bubble size distribution, or polydispersity, resulted a deviation of more than 5%, producing relatively less-uniform bubbles. Above the liquid flow rate of 33.34μL/s, gases did not form discrete bubbles, randomly dispersing through the liquid. Within the selected flow rates, discrete and uniform bubbles were produced with 1.2 and 2.5% variations (polydispersity index) of 134.62 and 79.52μm diameters, 17 and 10 bubbles/frame (for nitrogen gas), respectively. Within the selected liquid flow rate ranges, lower flow rates were mainly utilized for various types of experiments because they produce bubbles with larger size variations among different gases, resulting in clearer identification, as evidenced in Fig.6. Thus, the lowest liquid flow rate of 22.17μL/s was mostly adopted throughout the experiments otherwise noted differently.

Gas types vs. input energies:

Both flow rate and pressure of the gas streams were measured during the formation of gas bubbles to estimate required characteristic energy for the tested five gases. The gas pressure and flow rates were fixed at 13.10kPa and 3.33μL/s respectively, and the liquid flow rate was set as 22.17μL/s. The characteristic energy was estimated by multiplying the measured values of pressure and flow rate at the time of bubble formation.

Gas mixture ratios vs. bubble diameters:

Gas mixture ratios between the hypothetical target (CO_2) and carrier (N_2) gases were gradually varied from 0% to 100% in order to prove and establish the relationship between bubble volumes and the mixture ratios of multiple gases, while the diameters of the bubbles were monitored. The selected mixture ratios for CO_2:N_2 were 100:0, 80:20, 50:50, 20:80, and 0:100. Respective ratios were composed by discretely injecting CO_2 into pure N_2 based on volume. The pre-mixed gases were continuously injected by utilizing a high-precision syringe pump (KD Scientific KDS-130). The gas and liquid flow rates were fixed at 0.83 and 16.67μL/s, respectively. Note that this testing was performed by providing gas flows utilizing a syringe pump and resulted in a lower flow rate condition for bubble generation.

Characterization of a bubble gas sensor:

To validate the use of gas bubbles as a sensing element for a gas chromatography system, two preliminary experiments were carried out: (i) sensing of an injected target gas (C_5) from a GC system and (ii) sensor stability over time. For these experiments, a dose of pentane (C_5, specifically J.T. Baker 98% pentane) was injected in a flow of helium carrier gas through a commercial GC system (Thermo Scientific Focus GC). For all of the experiments here, gas pressure and liquid flow rates were set as 13.10kPa and 22.17μL/s, respectively, while the liquid phase was selected as a 52%w/w mixture of glycerol: water with a viscosity of 6.1mPa.s controlled by adding 2%w/w surfactant.

Gas (C_5) sensing:

To demonstrate the establishment of a chromatogram, a dip, or a sudden change, in bubble diameters, was monitored while injecting a target gas (C_5) of 0.01μL into a continuous flow of a carrier gas (He) at a flow rate of 1.00μL/s. The resultant bubble diameters were plotted across time to produce a chromatogram with the sudden peak or a dip. To identify a peak, a threshold in diameter change was set at two times the standard deviation from the baseline diameter (113μm) of helium (carrier gas) bubbles.

Overtime stability over time:

To observe the overtime stability of the bubble sensing mechanism, the pentane injection test was repeated over 67 times over a period of a month while the retention time, the peak location across the time-domain, was monitored. An identical pentane amount of 0.001μL was injected, while the location of the minimum bubble size was measured as the retention time. Since the retention time was subject to a tube length, the tube length was fixed as 270cm throughout the repeated experiments.

Results and Discussion:

The measurement results showed that (i) the volume of the gas microbubble uniquely depends on the gas types and mixture ratios, and that (ii) the monitoring of gas bubbles can be utilized as a gas sensor that produced a chromatogram and stable performance over repeated tests.

A. Characterization of bubble production:

Gas types vs. bubble volumes:

Experimental results showed that five types of gases (CO_2, He, H_2, N_2, and CH_4) produced respectively unique bubble volumes of 0.44, 0.74, 1.03, 1.28, and 1.42nL under identical flow conditions of gas pressure (13.10kPa) and liquid flow rate (22.17μL/s), indicating the existence of characteristic relationship between gas types and resultant volumes, as shown in Fig.5. The bubble volumes of He, H_2, N_2 and CH_4 were 68%, 134%, 191%, and 223% higher than that of CO_2, indicating a clear difference between each type of gas bubble and the CO_2 bubbles, as well as from each other. Note that these bubble volumes were calculated from the measured bubble diameters of 94.10 (CO_2), 111.90 (He), 125.09 (H_2), 134.62 (N_2), and 139.44μm (CH_4). Experimental results also showed that the five types of gases generated bubbles with low standard deviations of 0.085, 0.061, 0.054, 0.048, and 0.037nL and with low polydispersity indices (standard deviation of bubble diameters / average diameter ×100% [37]) of 6.19, 2.78, 1.75, 1.23, and 0.85% over approximately 8260 bubbles for a period of 1 minute, indicating high uniformity in the produced bubble sizes over time. It is noted here that typically a polydispersity index below 5% is accepted as uniform bubbles in microfluidic flow-focusing device research [35-37].

Gas types vs. p/q ratios vs. linearity:

Experimental results showed that (1) each gas type, CO_2, He, H_2, N_2, and CH_4, linearly increased in volume respectively with the increasing p/q ratios from 0.39 to 0.59kPaμLs^{-1}, from 0.14, 0.17, 0.23, 0.26, and 0.35 to 0.44, 0.74, 1.03, 1.28, and 1.42nL, and that (2) each gas type presented characteristic linear

coefficients (slope) of 1.38, 2.93, 3.45, 5.06, and 5.44nL/(kPa/μLs^{-1}), respectively (Fig.6). These results indicate the existence of characteristic volume expansion coefficients depending on gas types. The volumes of the produced bubbles were mostly distributed in the order of CO_2, He, H_2, N_2, and CH_4 within liquid flow rates between 22.17 and 33.34μL/s at a fixed gas pressure of 13.10kPa. As noted earlier, all the gases produced bubbles in uniform sizes within the selected flow range. Experimental results also showed that the volume discrepancies among gases increased at a higher p/q ratio, indicating easier gas identification at a lower liquid flow rate than a higher flow rate.

Gas types vs. input energies:

Figure 7 showed that each gas utilized characteristic amounts of energy to produce bubbles, including 0.20, 0.07, 0.15, 0.10, and 0.17mJ/s for CO_2, He, H_2, N_2, and CH_4, respectively, despite the identical supply of gas pressure and liquid flow rates of 13.10kPa and 22.17μL/s. The maximum and minimum required gas flow rates were measured as 0.50 and 2.34μL/s for He and CO_2, while the maximum and minimum required gas pressures were measured as 96.60 and 98.18kPa for CO_2 and H_2. The rest of the gases required pressure and flow rates inside these ranges. Measurement results also showed that the produced bubbles resulted in different volumes, as previously confirmed, of 0.44, 0.74, 1.03, 1.28, and 1.42nL for CO_2, He, H_2, N_2, and CH_4. The average energy required for each gas to generate bubbles during the period of 1 minute of bubble generation was calculated based on the equation $\frac{1}{t}\sum_0^t p(t)q_g(t)$, indicated by the parabolic dashed lines in Fig.7. It is notable that CO_2 required the highest amounts of energy despite the smallest resultant bubble volumes. The figure also showed that higher input energy tended to produce higher bubble volumes except for CO_2, which could be attributable to significantly higher solubility (more than 30 times greater).

Gas mixture ratios vs. Bubble diameters:

Experimental results showed that the different gas mixture ratios for CO_2:N_2 of 100:0, 80:20, 50:50, 20:80, and 0:100 (1) utilized characteristic energy amounts of 0.033, 0.047, 0.052, 0.061, and 0.077mJ/s, and (2) produced characteristic bubble diameters of 48.95, 77.99, 71.00, 78.53, and 99.50μm, as shown in Fig.8-(a). This required gas flow rate and gas pressure varied linearly from 0.29 to 0.84μL/s and 93.22 to 96.26kPa with the increasing mixture ratios. Measurement results also showed that (3) the resultant bubble diameters increased proportional to the mixture ratios, as shown in Fig.8-(b), indicating the feasibility of identifying the exact mixture ratios and volumes of each bubble in various sizes for known gas types. Fig.8-(b) shows that as the portion of N_2 increased in the CO_2/N_2 mixture from 0% to 100%, the produced bubble diameter increased from 48.95 (pure CO_2) to 99.50μm (pure N_2). The linear coefficient of the relationship, $d \propto km$ (d = bubble diameter and m = % of N_2 in CO_2), was measured as k

= 10.26μm/%, indicating 10.26μm diameter increase for every 1% addition of N_2 gas into CO_2/N_2 mixtures. This result validated the feasibility of predicting mixture ratios between the carrier gas and the target gas for a known gas by monitoring the diameter variations. Experimental results also showed that each mixture ratio for CO_2:N_2 produced uniform bubbles with polydispersity indices of 7.53, 3.38, 4.61, 3.77, and 1.92% except CO_2, which were calculated from 1054 bubbles for each mixture ratio. Note that this testing was performed at a unique flow condition utilizing a syringe pump, resulting in the average required input energy for CO_2 being lower than that of N_2 as well as gas pressure and flow rates for bubble generation.

B. Characterization of a bubble gas sensor:

The fabricated bubble gas sensor demonstrated the ability to (1) successfully generate a chromatogram by monitoring a train of the produced bubbles and (2) perform with stability and without degradation over time.

Gas sensing:

The bubble sensor demonstrated that a 0.01μL injection of pentane (C_5) into a continuous carrier gas stream of helium (He) was successfully identified by monitoring sudden reduction in the bubble diameters from 118.50μm of He bubbles (carrier) to 112.00μm by 6.50μm, which corresponds to 5.50% variation, over 25.35 seconds, as shown in Fig.9-(a). This result indicates the feasibility of the proof-of-concept bubble-based gas sensing. The retention time (the time period until pentane produced the minimum bubble diameter), was measured to be 119s, while the peak width was measured to be 4s, representing a chromatogram plate number of 29.8. The result also shows that the bubble size started to decrease at the 117^{th} second from the average diameter of 116.67μm to 112.00μm at the 120^{th} second as the minimum and then increased back to 120.63μm at the 122^{nd} second, forming a chromatogram peak. The minimum detectable volume was 0.002pL considering that the minimum detectable optical measurement limit was 1μm.

Fig.9-(b) shows that the resultant histogram from the injection of 0.10μL C_5 sample, containing 14,460 bubbles over the whole time period, clearly identified both He and C_5 bubbles in diameters. The average diameters of He and C_5 bubbles were measured to be 112.96μm and 105.02μm with the relative diameter difference of 7.94μm or 7.03%. Such a diameter difference was significantly larger than the standard deviation (2.01μm) from the diameter distribution of He bubbles by four times, allowing clear identification. The x-axis was divided into bin sizes of 0.35μm and approximately 3332 bubbles were counted for C_5 gas detection.

Stability over time:

Experimental results demonstrated that the bubble-based sensor produced stable retention time (peak occurrence time in the chromatogram) with variations of only 5.60% around the mean retention time of 92.40 second over 67 repetitive tests when tested with a tube length of 270cm, indicating performance stability over time unlike chemistry-based sensing mechanisms. Each test was carried out for 120-130 seconds and approximately 24,000 bubbles were utilized for image processing analysis. Note that the peak edges were determined when the measurement values changed beyond twice the standard deviation (5.60%) of helium bubble diameters without injection under a liquid flow rate of 1.00μL/s.

Conclusions:

We have developed a proof-of-concept microfluidic bubble-based gas sensor that demonstrated overtime stability for gas sensing application and was simple in structure and fabrication. The bubble-based gas sensor was fabricated by utilizing one mask in combination of polymer molding and bonding techniques. The fabricated device demonstrated that different gas types and binary gas mixture ratios produced characteristic bubble diameters while requiring characteristic energy levels, verifying the feasibility of identifying gases by monitoring bubble diameters. The resultant bubble-based sensor experimentally demonstrated the production of a gas chromatogram for the injection of a C_5 gas as well as long-term stability of the system as a gas chromatography system sensor.

Acknowledgement:

The authors are grateful to Hao-Chieh Hsieh for valuable assistance in GC operation. Fabrication was performed in the Utah nanofabrication facility at the University of Utah, Salt Lake City.

References:

[1] D. J. Brake, I. Fellow and G. P. Bates, "A guide to breathing rates in confined environments", *Technical article*.
[2] M. kampa, and E. Castanas, "Human health effects of air-pollution", *Environ. Poll.*, Vol. 151, pp. 362-367, 2008.
[3] M. Phillips, J. Herrera, S. Krishnan, M. Zain, J. Greenberg, and R. N. Cataneo, "Variation in volatile organic compounds in the breath of normal humans", *J. Chromatography B*, vol. 729, pp. 75-88, 1999.
[4] B. F. Yu, Z. B. Hu, M. Liu, H. L. Yang, Q. X. Kong, and Y. H. Lui, "Review of research on air-conditioning systems and indoor air quality control for human health", *Int. J. Refriger.*, Vol. 32, pp. 3-20, 2009.
[5] K. Wilkins, "Volatile organic compound from household waste", *Chemosphere*, Vol. 21, Iss. 1, pp 47-53, 1994.
[6] United States Environmental Protection Agency, http://www.epa.gov/otaq/toxics.htm
[7] H-C. Hsieh and H. Kim, "Miniature circulatory column system for gas chromatography", *Proc MEMS 14*.
[8] S. K. Kim, H. Chang, and E. T. Zellers, "Microfabricated gas chromatograph for the selective determination of trichloroethylene vapor at sub-parts-per-billion concentrations in complex mixtures", *Anal. Chem.*, 2011, **83**, 7198-7206.

[9] C. Lu, J. Whiting, R. D. Sacks, and E. T. Zellers, "Portable gas chromatograph with tunable retention and sensor array detection for determination of complex vapor mixtures", *Anal. Chem.*, 2003, **75**, 1400-1409.

[10] S. Reidy, D. George, M. Agah, and R. Sacks, "Temperature-programmed GC using silicon microfabricated columns with integrated heaters and temperature sensors", *Anal. Chem.*, 2007, **79**, 2911-2917.

[11] C. K. Ho, M. T. Itamura, M. Kelley, and R. C. Hughes, *Sandia Report*, 2001.

[12] D. Filenko, "Chemical gas sensors based on functionalized self-actuated piezo-resistive cantilevers", *PhD disst.*, 2009.

[13] D.-S. Lee, J.-K. Jung, J.-W. Lim, J.-S. Huh, and D.-D. Lee, "Recognition of volatile organic compounds using SnO_2 sensor array and pattern recognition analysis", *Sens. and Act. B*, Vol. 77, pp 28-236, 2001.

[14] E. Llobet, J. Brezmes, R. Ionescu, X. Vilanova, S. Al-Khailfa, J. W. Gardner, N. Barsan, and X. Correig" Wavelet transform and fuzzy ARTMAP-based pattern recognition for fast gas identification using a micro hot plate gas sensor", *Sensors and Actuators B*, Vol. 83, pp 238-244, March 2002.

[15] M. Penza, G. Cassano, and F. Tortorella, "Gas recognition by activated WO_3 thin-film sensors array", *Sensors and Actuators B*, Vol. 81, pp 115-121, December 2001.

[16] Complete list of VOC's: http://www.aqt.it/index.php?option=com_content&view=article&id=71&Itemid=107

[17] S. Bedair and G. Fedder, "Cmos mems oscillator for gas chemical detection", *Proc. IEEE Sensors*, 2004, 955-958.

[18] J. J. Whiting, C. S. Fix, J. M. Anderson, A. W. Staton, R. P. Manginell, D. R. Wheeler, E. B. Myers, M. L. Roukes, and R. J. Simonson, "High speed 2-D gas chromatography using microfabricated gc columns combined with nanoelectromechanical mass sensors", *Proc. Solid State Sensors Actuat. Microsyst. Conf. TRANSDUCERS Int.,* 2009, 1666-1669.

[19] M. Li, E. B. Myers, H. X. Tang, S. J. Aldrige, H. C. McCaig, J. J. Whiting, R. J. Simonson, N. S. Lewis, and M. L. Roukes, "Nanoelectromechanical resonator arrays for ultrafast, Gas phase chromatographic chemical analysis", *Nano Lett.* 2010, **10**, 3899-3903.

[20] S. I. Shopova, I. M. White, Y. Sun, H. Zhu, X. Fan, G. Frye-Mason, A. Thompson, and S. Ja, "On-column micro gas chromatography detection with capillary-based optical ring resonator", *Anal. Chem*, 2008, **80**, 2232-2238.

[21] R. P. Manginell, J. M. Bauer, M. W. Moorman, L. J. Sanchez, J. M. Anderson, J. J. Whiting, D. A. Porter, D. Copic, and K. E. Achyuthan, "A monolithically-integrated μGC chemical sensor system", *Sensors*, 2011, **11**, 6517-6532.

[22] S. J. Martin, G.C Frye, J. J. Spates, and M. A. Butler, "Gas sensing with acoustic devices", *Proc. IEEE Ultrasonics Symp.*, 1996, **1**, 423-434.

[23] P. R. Lewis, P. Manginell, D. R. Adkins, R. J. Kottenstette, D. R. Wheeler, S. S. Sokolowski, D.E. Trudell, J. E. Byrnes, M. Okandan, J. M. Bauer, R. G. Manley, and C. Frye-Mason, "Recent advancement in the gas phase microchemlab", *J. IEEE Sensors*, 2006, **6**, 784-795.

[24] S. Herberger, M. Herold, H. Ulmer, A. Burdack-Freitag, and F. Mayer, "Detection of human effluents by a mos gas sensor in correlation to VOC quantification by GC/MS", *Building and Environment*, 2010, **45**, 2430-2439.

[25] J. Liu, Y. Sun, D. J. Howard, G. Frye-Mason, A. K. Thompson, S. Ja, S. Wang, M. Bai, H. Taub, M. Almasri, and X. Fan, "Fabry-perot cavity sensors for multipoint on-column micro gas chromatography detection", *Anal. Chem.*, 2010, **82**, 4370-4375.

[26] K. Reddy, J. Liu, M. K. Khaing Oo, and X. Fan, "Integrated separation columns and fabry-perot sensors for microgas chromatography system" *J. Miroelectromech. Syst*., 2013, **22**, 11174-1179.

[27] K. Ferrara, R. Pollard, and M. Borden, "Ultrasound microbubble contrast agents: fundamentals and application to gene and drug delivery", *Annu. Rev. Biomed. Eng.*, 2007, **9**, 415-447.

[28] S. Huang, "Liposomes in ultrasonic drug and gene delivery", *Adv. Drug. Delv. Rev.*, 2008, **60**, 1167-1176.

[29] V. Srinivasan, V. K. Pamula, and R. B. Fair, "An integrated digital microfluidic lab-on-a-chip for clinical diagonostics on human physiological fluids", *Lab Chip*, 2004, **4**, 310-315.

[30] C. Muhlen, W. Khummueng, C. A. Zini, E. B. Caramao, and P. J. Marriott, "Detector technologies for comprehensive two-dimensional gas chromatography", J. Sep. Sci., vol. 29, pp. 1909-1921, 2006.

[31] S. Zimmermann, S. Wischhusen, J. Muller, "Micro Flame Ionization Detector and Micro Flame Spectrometer", *Sensors and Actuators B*, vol. 63, pp. 159-166, 2000.

[32] K. Cheung, L. Velasquez-Garcia, A. Akinwande, "Chip-Scale Quadruple Mass Filters for Portable Mass Spectrometry", *J. Microelectromech. Syst.*, vol. 19, pp. 469-483, 2010.

[33] S. Narayanan, B. Alfeeli, M. Agah, "Two-Port Static Coated Micro Gas Chromatography Column with an Embedded Thermal Conductivity Detector", *J. IEEE Sensors*, vol. 12, pp. 1893-1900, 2012.

[34] B. C. Kaanta, H. Chen, and X. Zhang, "Flow rate insensitive thermal conductivity detector", *Proc TRANSDUCERS' 11.*

[35] P. Garstecki, A. M. Ganan-Calvo and G. M. Whitesides, "Formation of bubbles and droplets in microfluidic systems", *Bull. Pol. Acad. Sci. Tech. Sci.*, 2005, **53**, 361-372.

[36] P. Garstecki, Irina Gitlin, Willow DiLuzio, and G. M. Whitesides, E. Kumacheva, and H. A. Stone, "Formation of monodisperse bubbles in a microfluidic flow-focusing device", *Appl. Phys. Lett.*, 2004, **85**, 2649-2651.

[37] P. Garstecki, H. A. Stone and G. M. Whitesides, "Mechanism for flow-rate controlled breakup in confined geometries: a route to monodisperse emulsions", *Phys. Rev. Lett*, 2005, **94**, 164501-1-4.

[38] A. M. Ganan-Calvo and J. M. Gordillo, "Perfectly monodisperse microbubbling by capillary flow focusing", *Phys. Rev. Lett*, 2001, **87**, 274501-1-4.

[39] P. Garstecki, M. J. Fuerstman, H. A. Stone and G. M. Whitesides, "Formation of droplets and bubbles in a microfluidic T-junction-scaling and mechanism of break-up", *Lab Chip*, 2006, **6**, 437-446.

[40] B. Dollet, W. Hoeve, J-P. Raven, P. Marmottant, and M. Versluis, "Role of channel geometry on the bubble pinch-off in flow-focusing devices", *Phys. Rev. Lett.*, vol. 100, pp 034504-1-4, 2008.
[41] T. Cubaud and C-M. Ho, "Transport of bubbles in square microchannels", *Phys. Fluids*, vol. 16, No. 12, pp. 4575-4585, 2004.
[42] M. J. Fuerstman, A. Lai, M. E. Thurlow, S. S. Shevkoplyas, H. A. Stone and G. M. Whitesides, "The pressure drop along rectangular microchannels containing bubbles", *Lab Chip*, 2007, **7**, 1479-89.
[43] T. Thorsen, R. W. Roberts, F. H. Arnold, and S. R. Quake, "Dynamic pattern formation in a vesicle-generating microfluidic device", *Phys. Rev. Lett.*, 2001, **86**, 4163-4166.
[44] R. Sun and T. Cubaud, "Dissolution of carbon dioxide bubbles and microfluidic multiphase flows", *Lab Chip*, 2011, **11**, 2924-28.
[45] T. Cubaud, M. Tatineni, X. Zhong and C. Ho, "Bubble dispenser in microfluidic device", *Phys. Rev. E*, 2005, **72**, 037302-1-4.
[46] T. Cubaud, M. Sauzade and R. Sun, "CO_2 dissolution in water using long serpentine microchannels", *Biomicrofluidics*, 2012, **6**, 022002-1-9.
[47] C. N. Baroud, F. Gallaire and R. Dangla, "Dynamics of microfluidic droplets", *Lab Chip*, 2010, **10**, 2032-45.
[48] B. J. Adzima ans S. S. Velankar, "Pressure drops for droplet flows in microfluidic channels", *J Micromech. Microeng.*, 2006, **16**, 1504-10.
[49] T. Ward, M. Faivre, M. Abkarian and H. A. Stone, "Microfluidic flow focusing: drop size and scaling in pressure versus flow-rate-driven pumping", *Electrophoresis*, 2005, **26**, 3716-24.
[50] A. Bulbul, A. Basu and H. Kim, "Characterization of microbubbles in of multiple gases in microfluidic channels", *Proc μTAS 13.*
[51] A. Bulbul, H-C. Hsieh and H. Kim, "Microfluidic bubble-based gas sensor", *Proc MEMS 14.*
[52] P. S. Epstein, and M. S. Plesset, "On the stability of gas bubbles in liquid gas solution", *J. Chem. Phys.*, Vol 18, pp 1505-1509, 1950.
[53] A. Kabalnov, D. Klein, T. Pelura, E. Schutt, and J. Weers, "Dissolution of multicomponent microbubbles in blood stream: 1. Theory", *Ultrasound in Med. & Biol.* Vol 24, no 5, pp 739-749, 1998.
[54] A. R. Prakash, S. Adamia, V. Sieben, P. Pilarski, L. M. Pilarski, and C. J. Backhouse, "Small volume PCR in PDMS biochips with integrated fluid control and vapor barrier", *Sens. and Act. B*, Vol 113, pp 398-409, 2006.
[55] http://encyclopedia.airliquide.com/encyclopedia.asp
[56] E. L. Cussler, "Diffusion: Mass transfer in fluid systems (2nd ed)", New York, Cambridge University Press, ISBN 0-521-45078-0.

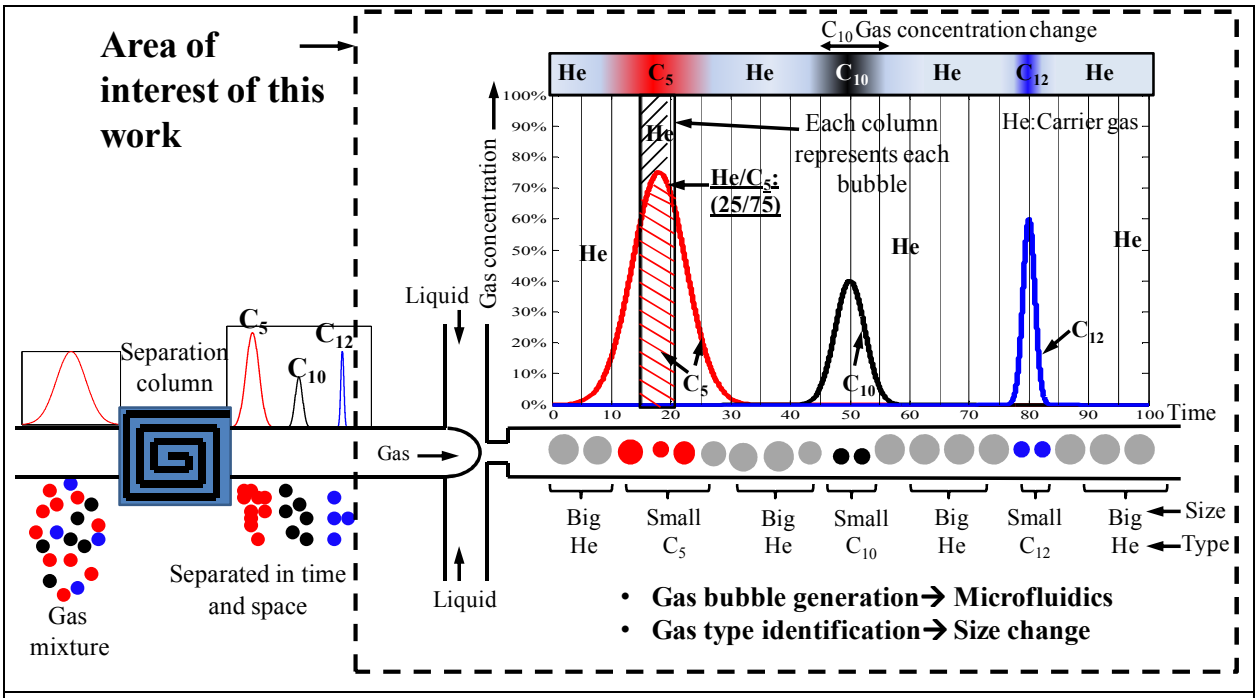

Figure 1: Concept of gas sensing: (from left to right) gas mixture passes through separation column and separated as individual component (C_5, C_{10}, C_{12}). The carrier gas is helium and it forms trains of uniform sized bubbles in a microfluidic flow-focusing device. The device changes the size of bubbles when the gas changes from helium to another (He:sample (C_5/C_{10}/C_{12}) mixture). By monitoring the size change of bubbles the device enables to generate chromatogram.

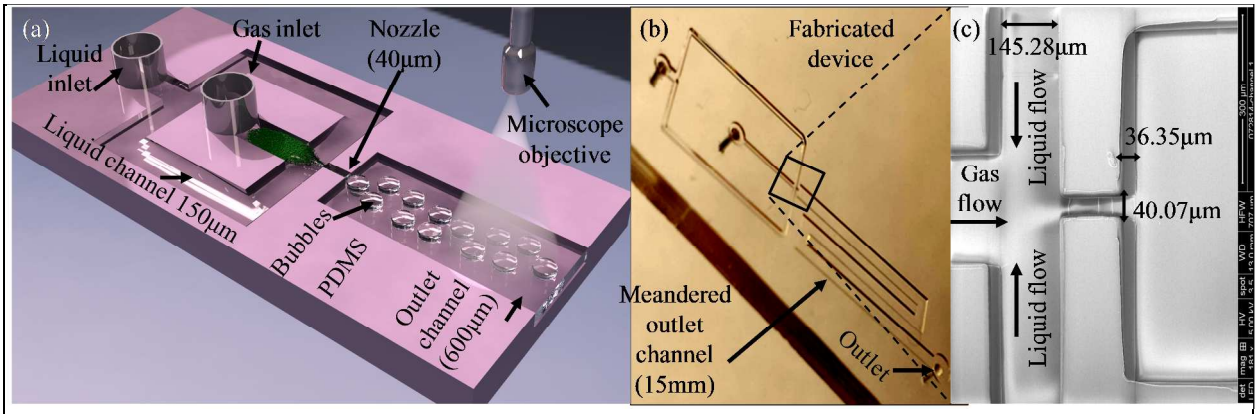

Figure 2: Device structure: (a) a microfluidic flow-flowing device showing liquid and gas channels to make trains of bubbles, (b) device photo, and (c) SEM image of nozzle section showing nozzle, channel height, gas channel and liquid channel.

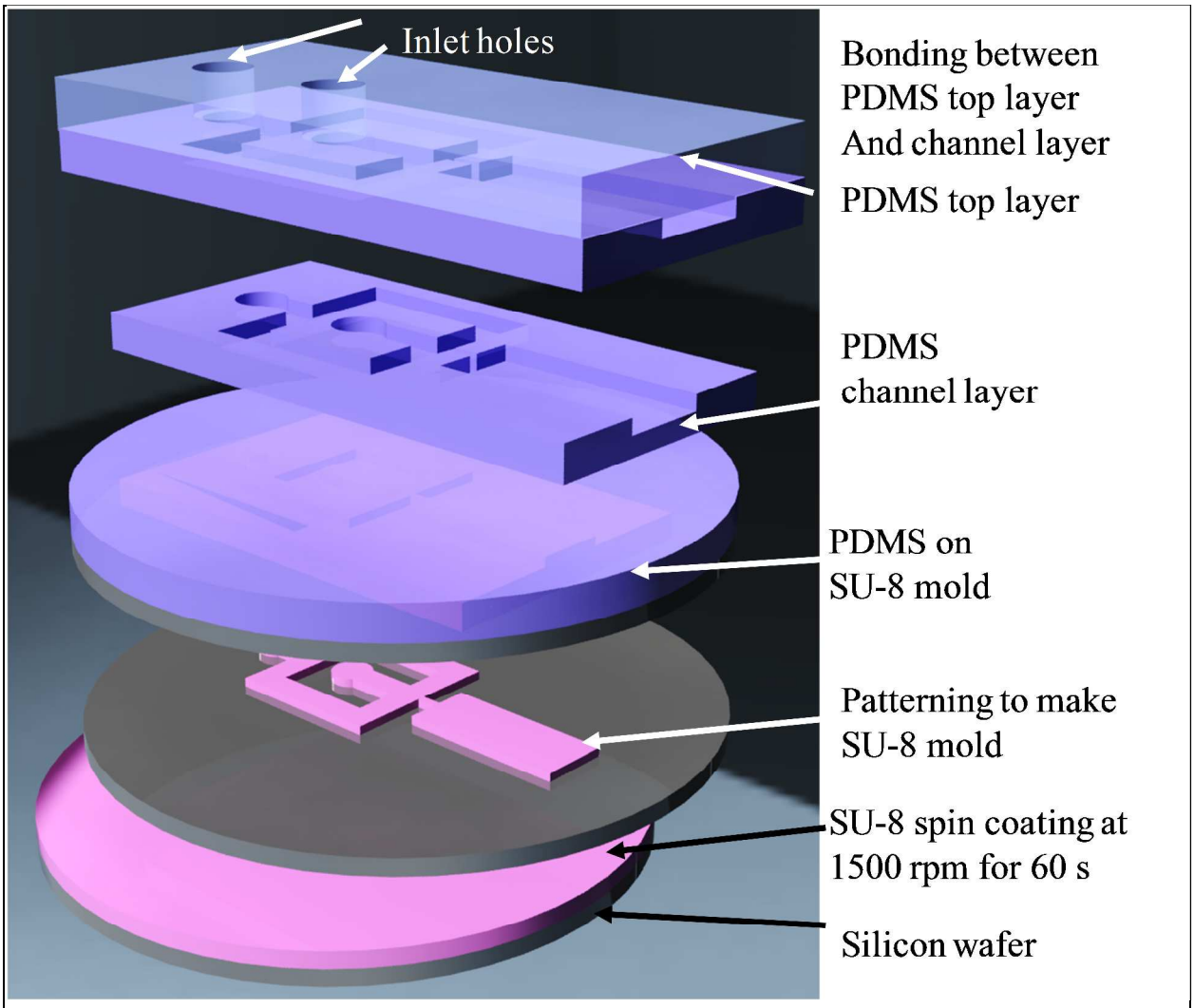

Figure 3: Fabrication process flow of the microfluidic flow-flowing device.

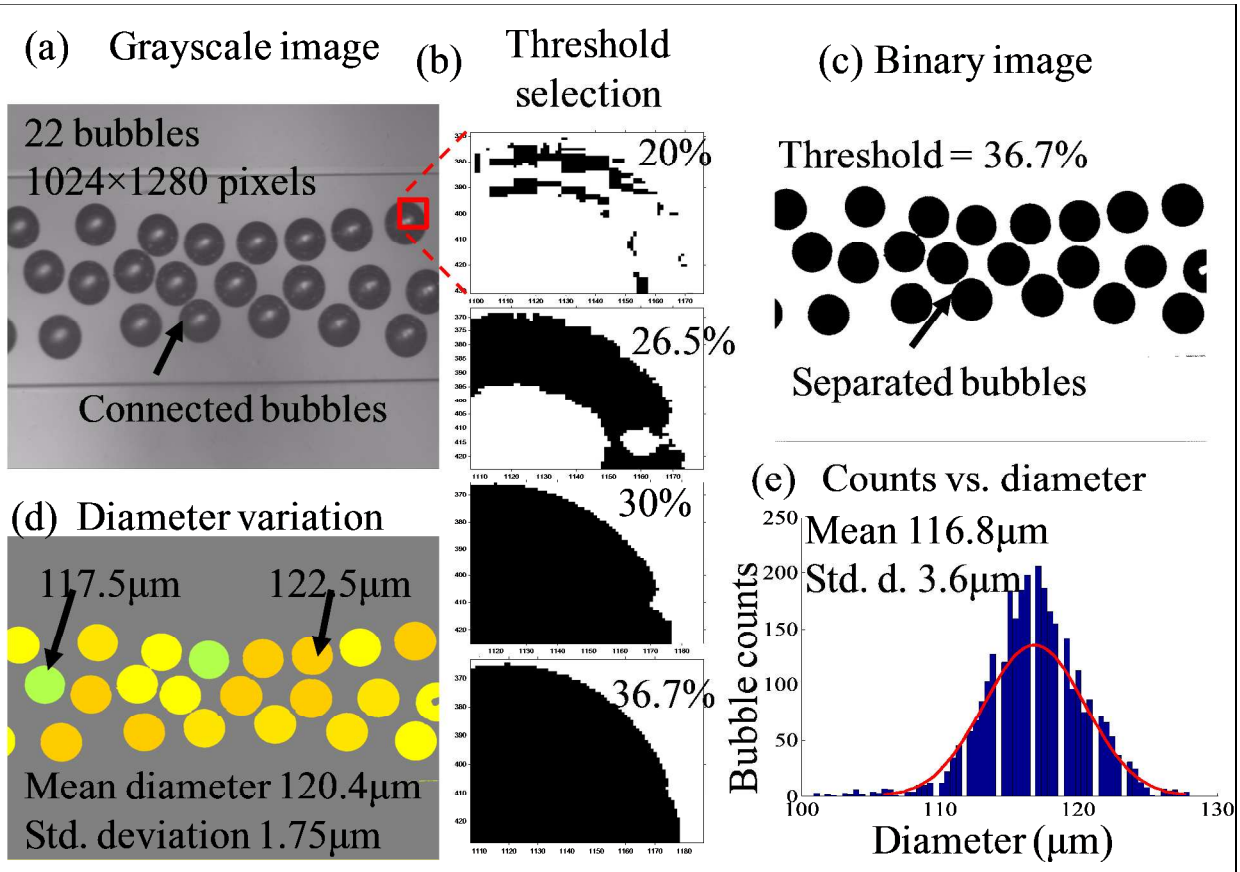

Figure 4: Image processing technique (a) one grayscale frame from a video, (b) threshold selection criteria, (c) conversion to binary image, (d) diameter measurement and color labeling, and (e) statistical distribution of bubble counts over the total diameter variation in 10s.

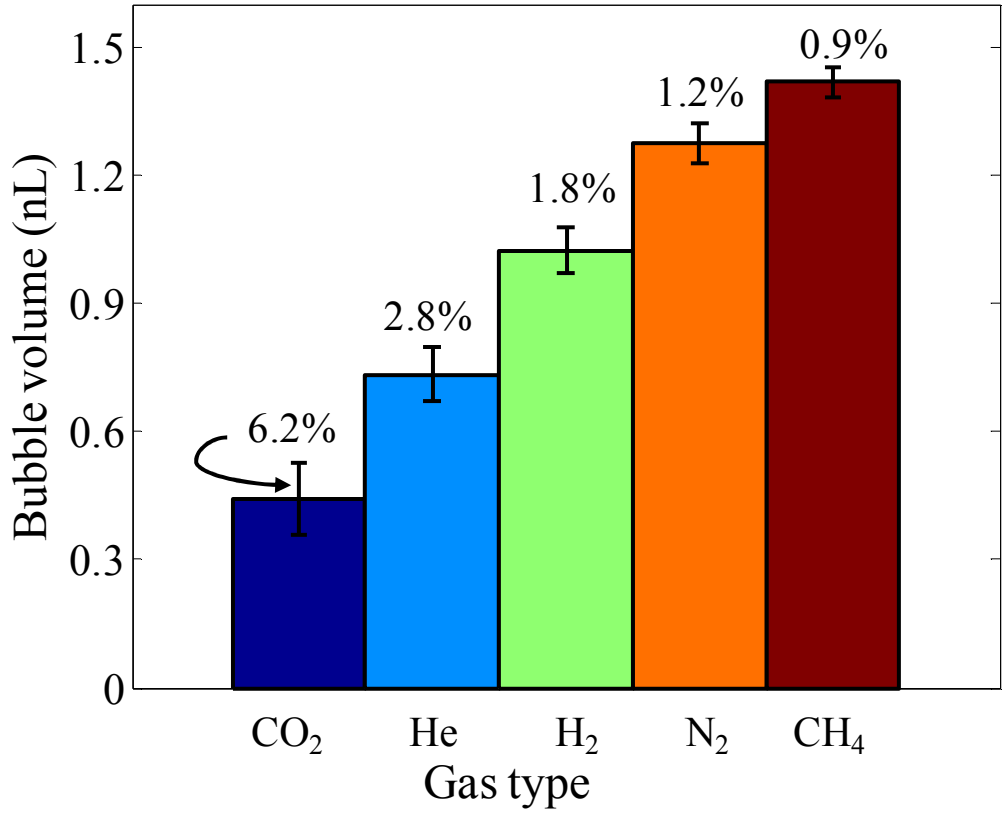

Figure 5: Gas types vs. bubble volumes: variation of gas bubble volume of five different gas types (CO_2, He, H_2, N_2, and CH_4) at gas pressure of 13.10kPa, liquid flow rate of 22.17μLs^{-1} and liquid viscosity of 6.10mPa.s, showing how bubble size changes according to the gas types.

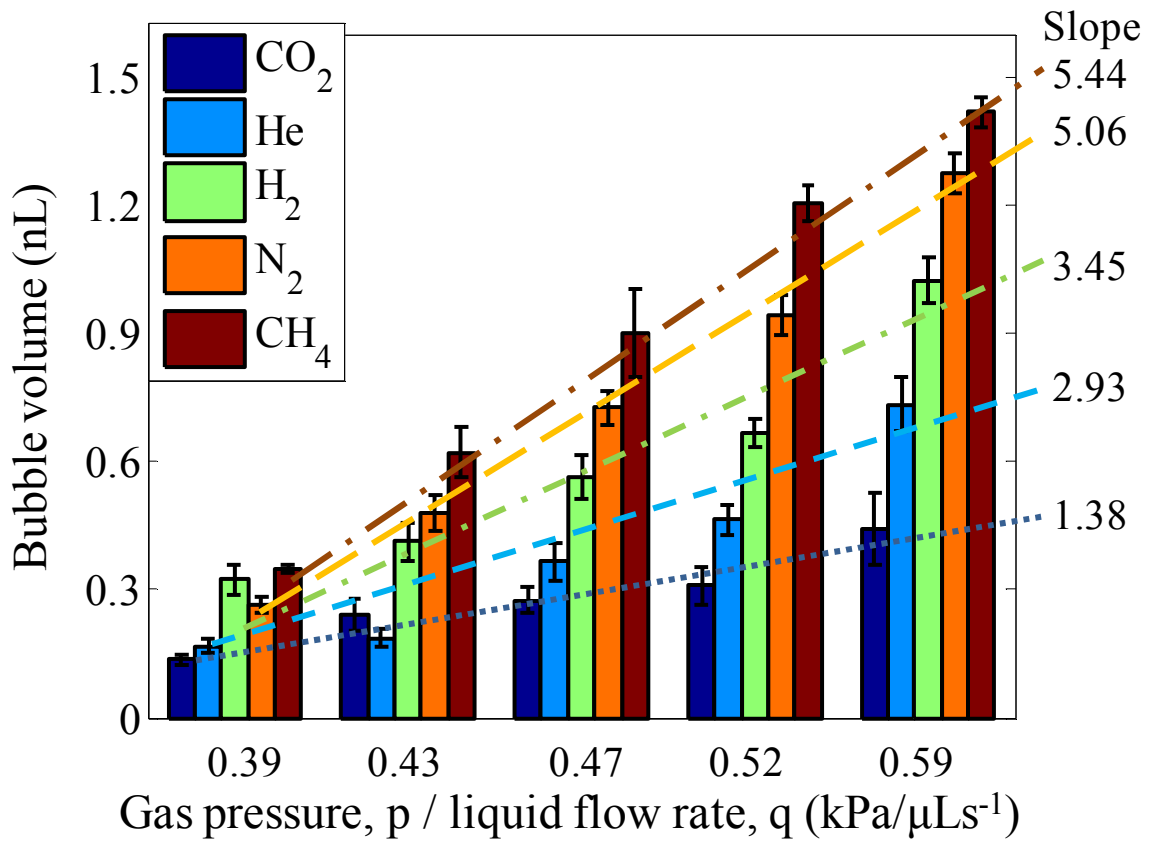

Figure 6: Gas types vs. bubble volume vs. linearity: variation of bubble volume from one gas to another at different p/q ratios showing different linearity coefficients (slope) for each gas.

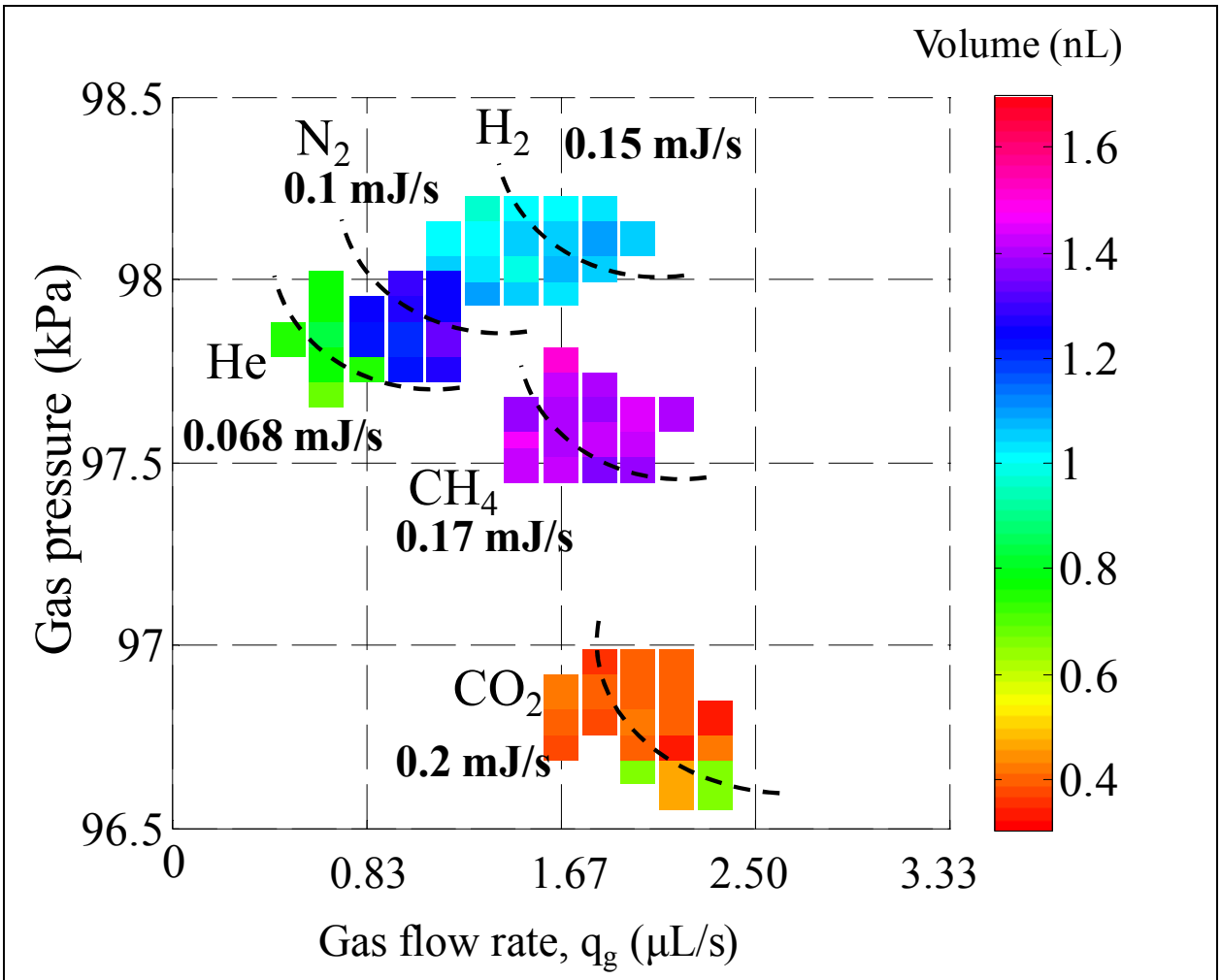

Figure 7: Energy correlation with respect to required amount of gas pressure, gas flow rate and bubble volume indicating each gas required characteristic amount of pressure and flow rate to make characteristic volume of bubbles.

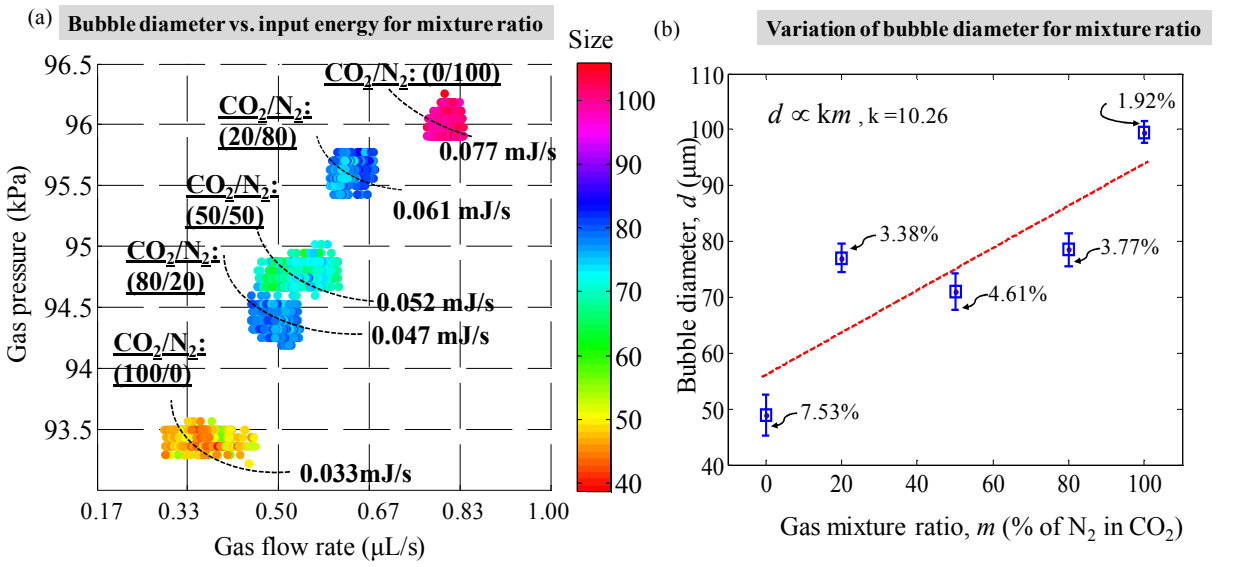

Figure 8: Correlation of characteristic energy and bubble diameter with gas mixture ratio: (a) required gas pressure, gas flow rate and hence, the required amount of energy is proportional to the N_2 and CO_2 mixture ratio, (b) each mixture produce bubbles where the bubble size is linearly related to the mixture ratio.

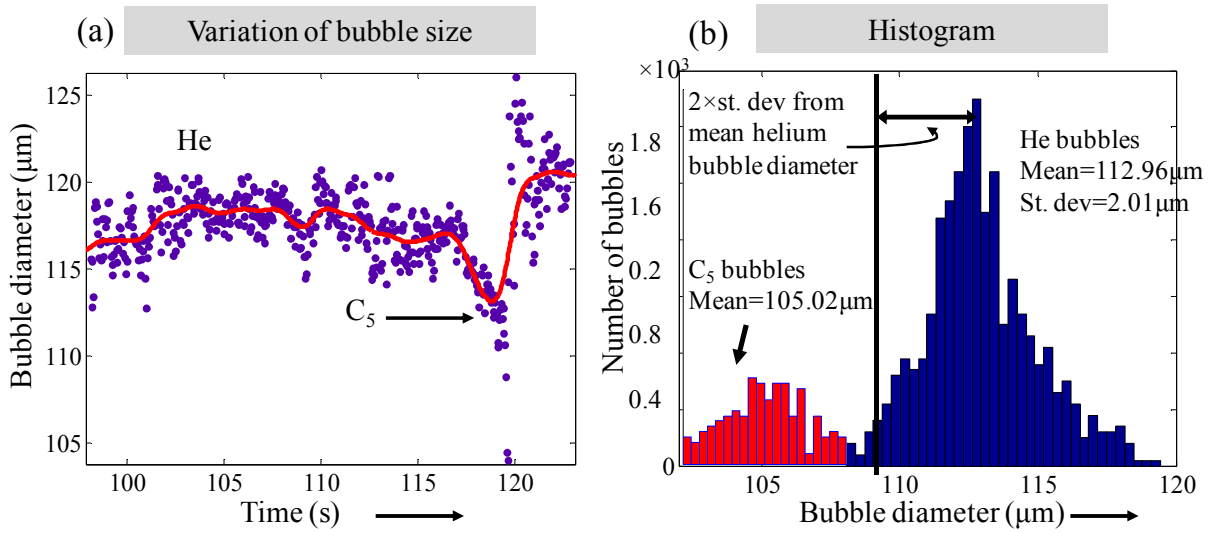

Figure 9: Bubble size variation for C_5 injection: (a) bubbles sharply reduce their diameter when the device experiences a transition from helium gas to C_5 gas, (b) histogram of bubble size over whole time period shows a clear difference between the helium and C_5 bubble indicates presence of C_5 in helium flow.

Table 1: Comparison of different gas sensors.

	Physics-based gas sensors				Chemistry-based gas sensors				
	Bubble (Proposed)	**TCD** [33-34]	**MS** [32]	**FID** [31]	**Chem-R** [17-18]	**SAW** [21-22]	**MOS** [23-24]	**F-P** [25-26]	**Resont.** [19-20]
Output	Stable	Stable	Stable	Stable	Drifting	Drifting	Drifting	Drifting	Drifting
Miniaturization	Possible	Possible	Impossib. (vacuum)	Impossib. (ionizer)	Possible	Possible	Possible	Impossib. (laser)	Impossib. (vacuum)
Fab.	Simple	Complex	Complex	Complex	Simple	Simple	Medium	Medium	Medium
Sample	Intact	Intact	Damaged	Damaged	Intact	Intact	Intact	Intact	Intact
Post-analys.	Possible	Impossib.	Impossib.	Impossib.	Impossib.	Impossib.	Impossib.	Impossib.	Impossib.

Table 2: Solubility, solubility normalized by density and diffusivity of some gases in pure water [55-56].

	CO_2	He	H_2	N_2	CH_4
Solubility (vol/vol)	1.7160	0.0090	0.0200	0.0230	0.0540
Solubility/density (g^{-1})	0.9178	0.0532	0.2512	0.0198	0.0794
Diffusivity (cm^2/s)×10^{-5}	1.9200	6.2800	4.5000	1.8800	1.4900